SURFACE REGISTRATION USING TEXTURED POINT CLOUDS AND MUTUAL INFORMATION

By

Tuhin Kumar Sinha

Thesis

Submitted to the Faculty of the

Graduate School of Vanderbilt University

in partial fulfillment of the requirements

for the degree of

MASTER OF SCIENCE

in

Biomedical Engineering

December, 2002

Nashville, Tennessee

Approved by:

Michael I. Miga

Robert L. Galloway

ACKNOWLEDGEMENTS

I would like to thank my advisors for their guidance while completing this thesis. I would specifically like to thank Dr. Galloway for his support before and during my career as a graduate student. I would also like to specifically thank Dr. Miga for his diligence and patience in working with me.

I would like to acknowledge the support of the many lab members that I have known in SNARL and BML. Specifically, Andy Bass, Mark Bray, David Cash, Steve Gebhart, Steven Hartmann, Jim Stefansic, and Chad Washington.

Finally, I would like to thank my family and friends for their support during this process. Specifically, Ashnil Chopra, Chad Grout, Agnella Izzo, Bryan Martin, Neal Massand, Dana Powers, Sandy Rathor, my parents and my better half, Tanoy Sinha, my brother.

TABLE OF CONTENTS

Page

LIST OF TABLES

LIST OF FIGURES

CHAPTER I

INTRODUCTION

An emerging area of research within image-guided procedures (IGP) is deformation tracking and model-updated IGP. Research in this area is aimed at augmenting current IGP for greater intra-operative efficacy and accuracy. As a comment on current surgical protocol, Galloway states that "a surgeon puts up his pre-operative images on a light box, gathers the information he needs, then turns his back and does the surgery." [2] There are two concerns with this approach: (1) the surgeon is relying on his or her memory for target planning during surgery, and (2) the surgeon is relying on out-dated patient data for target planning. IGP can be used to address the first concern, that is, an interactive system can be used to quantitatively involve the pre-operative image sets during surgery. Thus, the physician quantitatively locates positions in the image in real-time, which relieves dependence on memory-based therapy targeting. The second concern is the focus of much research in extending IGP systems. More specifically, this area of research is developing strategies to update the shapes defined by pre-operative images *during* surgery to reflect conditions in the operating room. The work of this thesis takes initial steps at incorporating the data taken in the operating room into IGP for neurosurgery. A unique surface registration algorithm is introduced that allows patient-to-image registration of the data generated by a laser scanner. This registration provides the ability to easily and accurately measure changes in the brain's surface during surgery for model-updated IGP.

I.1 Image-guided Procedures

IGP are defined as procedures that use pre-operative datasets (3-D images) quantitatively to guide the surgical process[3]. The central component of any IGP concerns how accurately one can register the patient during surgery to his/her patient-specific three dimensional datasets. Registration establishes the relationship (i.e. mathematical mapping) between the intra-operative coordinate system (physical-space) and the pre-operative image coordinate system (image-space). This pro-

cess allows the physician to map intra-surgical positions to the most appropriate position in image-space, i.e. stereotaxy.[1]

Several methods have been developed to provided accurate stereotaxy. The first attempts to register physical-space to image-space were taken by Horsley and Clarke [4] applied to non-human subjects. Their method employed a rigid frame affixed to anatomical landmarks. The position of a probe attached to the frame was then precisely resolved relative to the anatomical points. Subsequent stereotactic frames expanded on this theme and applied their techniques to human subjects [5]. Crucial to the method of stereotaxy using frames was the rigidity of the frame to the patient's anatomy. That is, positions of the patients anatomy relative to the frame are fixed in both image-space and physical-space. Researchers realized that this rigidity could be maintained without using cumbersome frames, thus leading to the development of frameless stereotaxy. The most common method of frameless stereotaxy involves rigid markers in both image-space and physical-space, localization of the markers in each space, and a point-based registration of the markers. Rigidity here implies that the distances between markers are preserved between spaces. Initially intrinsic (anatomic) markers, such as bony structures on the face, were used for frameless stereotaxy [6]. However, difficulty in accurate localization limited their widespread adoption for IGP. A group at Vanderbilt University thoroughly researched the localization errors associated with markers in different imaging modalities and physical space, their work has lead to the development of highly accurate extrinsic markers (Acustar®) for use in IGP [7]. For stereotaxy, the centroids of the Vanderbilt markers are localized in image-space and physical space. In image-space, localization is performed either manually, or automatically using standard image processing techniques. In physical-space, the markers are localized using either optical, electromagnetic or acoustical methods, with optical methods being the most accepted [6]. Once the markers have been localized in each space, the mapping between them is found as a solution to the Orthogonal Procrustes' Problem (OPP). This process is often called a point-based registration [8]. The mathematical formulation of this problem and its solution are discussed later. This protocol for frameless stereotaxy (i.e.

[1]From the Latin: *stereo* = three dimensions, *tactus* = to touch.

using extrinsic markers and point-based registration) has become the *de facto* method of stereotaxy for IGP.

However, rigid extrinsic markers and point-based registrations are limited in the information they provide. In the case of neurosurgery, they are attached the to the skull, not the brain. Thus, the registration provided is not relative to the organ of interest. Furthermore, the registration provided using point-based systems are affected by the number and placement of markers in each modality. Too few markers lead to inaccurate registrations and poorly placed markers result in ineffective registrations [9]. Finally, point-based registrations are not retro-active. That is, soft-tissue deformations, e.g. brain deformations in neurosurgery, are not resolved by this registration protocol, the implications of which will be discussed in the next section. Nonetheless, point-based registrations and extrinsic markers for IGP provide improved therapy planning and intra-operative targeting, and are essential to current IGP.

I.2 Model-updated image guided procedures

Recent studies have reported the need for organ shift compensation strategies to further improve IGP navigation [10][11]. Kelly et al. initially reported brain deformation (shift) during stereotactic procedures [12]. The shifting of the brain during stereotactic procedures occurs due to a variety factors including swelling, pharmacological agents, physiology, and the therapy itself. Nimsky et al. have quantified deformations in the brain to be on the order of millimeters for deep tissue and centimeters for surface tissue, thus, showing the quantitative effect of shift is significant given that submillimetric accuracies are desired for surgery [11]. Reconciling the differences between the intra-operative reality and the pre-operative images is referred to as image-updated IGP [13]. Some research groups, i.e. Nabavi et al. and Nimsky et al., compensate for organ shift by using intra-operative imaging devices [14]. Within these frameworks the intra-operative data acquisition and image-update happen concurrently. Some groups have researched intra-operative CT as an intra-operative image acquisition, but logistical concerns, including dose, have limited its adoption for intra-surgical use [15]. Registered intra-operative ultrasound has also been developed for IGP [16]. However, poor image quality and degradation of tissue contrast over the course of a surgical

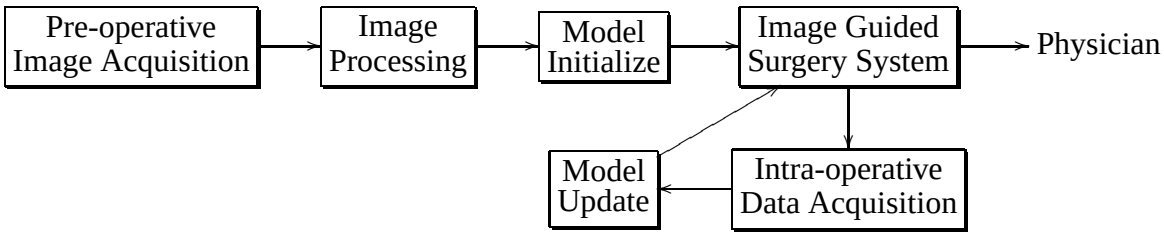

Figure I.1: Model-updated image guided surgery data pipeline.

procedure limit its effectiveness. Nimsky et al. have reported successful implementation of image-updated IGP using intra-operative magnetic resonance imaging (iMR) and show millimetric target accuracy results for this method in the brain [17]. They go on to report that out of 145 patients subjected to IGP in the brain, only 14 required image-updating during surgery. This observation, along with the high cost and difficult implementation of iMR, question the overall efficacy of iMR as a tool for image-updated IGP.

More available methods of image-updated IGP have been proposed recently [18]. These methods rely on physical or statistical models to update pre-operative data in the operating room. A schematic representation of the model-updated IGP pipeline is shown in Figure I.2. The intra-operative data collected provides constraints for the update model. For example, in a physical computational model of the brain, surface characteristics provide boundary conditions [19]. For statistical models, surface movements provide similar constraints [20]. This thesis focuses on the link between intra-operative surface data acquisition and model-updating for the IGP data pipeline. Specifically, the aim is to observe cortical surface characteristics during surgery and reflect those observations in a computational model. Thus, the intra-operative data collected is used in conjunction with pre-operative data for the IGP. This is in contrast to the methods described by Nimsky and Nabavi and does not produce the ground truth results observed by them. However, the implementation details for a computational approach are somewhat less complicated. Patient transport during surgery is not needed, as described by Nimsky, and constraining the range of movement of the surgeon is also not necessary as in the case of the “double-donut” intra-operative magnetic resonance unit used by Nabavi. Furthermore, advancements in numerical modeling of the brain will hopefully reduce the residual error between the two methods.

A necessity in any model-updated IGP is characterization of intra-surgical conditions, many methods have been explored to provide an accurate and efficient characterization. Intra-operative data has been acquired during surgery using: A-mode ultrasonography [21] and tracked palpation [22] for surface characterization, tracked endoscopy for characterization of internal structures [23], B-mode ultrasound for deep tissue visualization [24], laser spectroscopy for quantification of deep tissue properties [25][26], and electrical stimulation for localization of eloquent areas of the brain [27]. Thus, there is a wealth of intra-operative data that can be acquired and used within a model-updated image-guided procedure. There is a subtlety to model-updated IGP that is worth recognizing; the model-updating pipeline can accommodate not only anatomical changes, but physiological changes as well. In fact an ultimate goal of model-updated IGP is reflecting both anatomical *and* physiological changes in the operating theater [17]. All of the aforementioned methods of intra-operative data acquisition provide raw data for the model-updating pipeline.

This thesis uses a laser range scanner (LRS) for novel characterization of the cortical surface for model-updated IGP. In addition to laser triangulation of the surface, the scanner also reports texture map coordinates [28] for each triangulated point. The texture coordinates allow scalar values from a CCD image acquired during the scan to be associated with each point in the cloud. The hypothesis here is that the textured point cloud captured during surgery will contain both cortical sulcal and vessel patterns that can be used to register the patient to their pre-operative images. Using features from the cortical surface for registration does have precedent. Nakajima et al. demonstrated a target registration error of 1.3 ± 1.4 *mm* using projected cortical vessels from video images for registration [29]. More recently, Nimsky et al. reported a deformable surface approach to quantify surface shifts using a variation on the iterative closest point (ICP) algorithm [11]. Also, some preliminary work using a scanning based system for cortical surface registration has been reported but a systematic evaluation has not been performed to date [30]. The novelty of the approach reported here is that both vessel information and three-dimensional geometry is used as the basis of alignment. Furthermore, the scanner provides a highly accurate method for tracking the brain surface that will also serve as a valuable source of input data to a model based brain shift

compensation strategy.

I.3 Surface Registration and Mutual Information

As an initial step in the registration approach, an implementation has been developed using an iterative closest point (ICP) [31] framework with mutual information (MI) [32]. The iterative closest point algorithm (ICP), first postulated by Besl and McKay[31] is a well understood and documented strategy for surface alignment. Building on the point-based registration technique described earlier, the heart of the algorithm lies in the solution of multiple (OPP)[8]. The general form for the (OPP) is given in Equation I.1.

$$AT = B + E \tag{I.1}$$

where A and B are given and an orthogonal T ($TT^T = I$)[2] is desired to minimize the trace,

$$\min\left(EE^T\right) = \min\left((AT - B)(AT - B)^T\right) \tag{I.2}$$

Mathematically, the solution of the problem transforms matrix A into B via T, with the trace representing the residual error in alignment. For the canonical basis set (x,y,z) used in this paper, the 4x4 matrix T can be separated further into a translation and rotation component (see Equation I.3).

$$T = R + D \tag{I.3}$$

where R is an orthogonal rotation matrix, and D is the translation matrix. Arun found a solution for the rotational component of T using singular value decomposition methods (SVD)[33] that is used in this thesis. The translation component to the transformation (T) is found trivially and independently of the rotation component. Arun's method is expressed systematically in the methods section. Nonetheless, this conceptual solution is easily applied to medical image registration. For fiducial registrations, A and B represent the two sets of corresponding fiducials and T represents

[2] In this thesis, uppercase E represents a matrix and lowercase $\vec{e}$ represents a vector.

the transformation of coordinates in physical space to imaging space (or vice versa). For ICP, each iteration of the algorithm creates point set correspondence using a closest distance metric between points in the two clouds. The transformation relating the corresponding point sets found as a solution to a Procrustes' problem and the process is repeated. The algorithm ends when a predetermined distance metric has been optimized, usually the mean closest Euclidean distance (mean L_2 norm)[3]. A limitation of ICP, when applied to cortical surface registration, lies in the geometry of the cortex. The hemispherical shape of the cortical surface creates many orientations that are valid solutions for ICP. Thus, in a least-squared distance sense, the points in two point clouds might register well with ICP without correct orientation.

Information theory as applied to medical image registration can be used to overcome this limitation for cortical surfaces. A way to measure the mathematical information content within a signal was originally proposed by Claude E. Shannon in his landmark paper "A Mathematical Theory of Communication"[4][34]. Referred to as the Shannon entropy (see Equation I.4 for the entropy of a continuous signal and I.5 for the entropy of a discrete signal), this measure used the transition probabilities of random variables in a signal to ascertain the information content within the signal.

$$H(x) = K \int_{-\infty}^{\infty} p(x) \log p(x) dx \tag{I.4}$$

$$H(x) = K \sum_{i} \hat{p}(x_i) \log(\hat{p}(x_i)) \tag{I.5}$$

where $p(x)$ is the probability density function of the signal x and K is any scalar value[5]. As a simple example, the entropy of a signal whose transitions are precisely known (that is, the signal can be analytically characterized) has an entropy of 0. For a signal whose transition probabilities are distributed equally over the range of the signal the entropy is equal to 1. Although the entropies in I.4 and I.5 are written as functions, the random variable in parentheses is used as a label. Mathe-

[3]Other distance metrics can also be used in ICP, e.g. L_1, L_∞ for real coordinates or "cityblock" distances for integer coordinates, and the RMS distance maybe substituted for the arithmetic mean.

[4]The paper was later renamed "*The* Mathematical Theory of Communication".

[5]K is usually used to put the entropy in terms of physical quantities.

matical entropies are always scalar, and thus $H(x)$ should not be interpreted as a function of x. This labelling convention follows that of Shannon and is used throughout this thesis. Novel uses for entropy were proposed by Shannon including the information carrying capacity of communication channels and information generation rates of communication channels.

Hawkes and Hill were the first to apply entropy and information theory to medical imaging registration [35]. However, Viola and Wells, and Collignon independently introduced an extension to Shannon's initial work that allowed an accurate and robust method for registering a surface [32][36][37]. Called Mutual Information (MI), MI approximates the similarity in information between two random variables using both the marginal and joint entropies of the random variables. A modification to the standard measure of MI, called Normalized MI (NMI), was proposed by Studholme [38]. Registration of inter-modality medical imaging volumes showed that NMI proved more robust than conventional MI. For this reason, NMI values were used in this paper. NMI can be written concisely as follows,

$$NMI(x,y) = \frac{(H(x)+H(y))}{H(x,y)} \tag{I.6}$$

for a discrete random variable x. As written I.6, the registration becomes a problem in optimizing NMI for a global extremum. The specific implementation of the registration process used in this thesis is discussed in the methods section.

Although ICP and MI have been used extensively [39][40], previously published registration frameworks do not entirely apply to the unique data provided by the scanner or this particular registration approach. The data acquired by our scanner will allow for a one to one correspondence between contour point and image intensity, i.e. the need to create an image from the three-dimensional surface is not necessary. However, intensity correspondence between a three-dimensional MR surface and an intra-operatively acquired laser-scanned cortical surface is somewhat more elusive. ICP may provide an adequate correspondence but this is an area that is actively being investigated in the approach. The most similar work relating to this registration framework is that by Johnson and Kang [41] in which these investigators used an objective function for reg-

istration based on a combined Euclidean distance and color difference metric. Used primarily in a landscape alignment application, this technique would not be amenable to the alignment process here, since the intensity distribution between scanner and MR image data is fundamentally very different. No registration algorithm has been developed that will register textured three-dimensional surfaces from two different imaging modalities within the context of cortical surface registration as presented in this thesis.

CHAPTER II

METHODS

Algorithms for textured surface generation and registration in physical space and imaging space are explored in this chapter. For model-updated IGP textured surfaces in the physical world are registered to the pre-operative images taken before surgery. These registered datasets allow for the application of physical models to the pre-operative datasets for improving guidance during surgery. The following sections outline how each type of surface is generated and the registration algorithm used in the experiments.

Before outlining the algorithmic methods used in this thesis, an introduction to the Visualization toolkit (VTK) is useful. VTK, or The Visualization Toolkit (Kitware Inc.) provided the data object framework used in this research. The research and literature on computer graphics and visualization is extensive, however, the research goals are relatively few and easy to understand. One of the most compelling topics is the efficient and accurate display of multi-dimensional objects on a two-dimensional screen [28]. To simplify this task the open graphics library (OpenGL, www.opengl.org) was created, which provides a standardized computer graphics rendering pipeline for multi-dimensional data visualization. Abstracting a layer above OpenGL (the Open Graphics Library, Silicon Graphics Inc.), VTK provides a C++ class based approach to handling multi-dimensional datasets for computation and visualization. VTK allows an easily extensible interface for multi-dimensional data objects. All objects are manipulated in the VTK framework before being passed to OpenGL for rendering. Data objects in VTK can be split into two categories. The first, handles the geometry and topology of datasets. Briefly, in VTK the geometry of a dataset reflects the 3 dimensional location of points and vertices; and the topology reflects the relationship between (i.e. connections) points and/or vertices. The second category of data represents a list of attributes of the geometry dataset, including: scalar values, vector values, texture map coordinates, normals, tensors, etc. Furthermore, VTK defines a framework for process objects that can be used to generate or filter VTK datasets and their attributes. Finally, VTK's in-

put/ouput process object design allows for building on previously designed algorithms and linking them together to create very intricate algorithms. This feature, along with its extensibility, existing code-base, and mature API determined the use VTK for data management and manipulation in this thesis.

II.1 Textured Surface Generation

A laser scanner system (RealScan 3D, 3D Digital Corporation, Danbury, CT) capable of capturing three-dimensional topography as well surface texture mapping to sub-millimeter accuracy was utilized (see Figure II.1) to generate phantom textured data from a ball. Laser range scanning, or laser triangulation, builds on the *Law of Sines* (see Figure II.2 and Equation II.1). The distance between transmit and receive points, the separation distance d, was known in the scanner. Also the emission angle, b, and reflection angle, a were known. From these quantities and Equation II.1, the range distance r was calculated. For the laser scanner used in this thesis, the transmit signal was a laser pulse that was diffracted and guided using a pivoting mirror. The receiver was a CCD grid that detected the reflection of the laser light from the surface of interest. The scanning field consists of 500 horizontal by 494 vertical points per scanline and was accomplished in approximately 5 seconds. Extensive calibration and characterization has been performed by Cash et al. and has demonstrated the fidelity at which surface data can be acquired [42]. They have shown repeatability in scanning a Teflon ball (diameter: 25.40 *mm*) on the order of 0.05 *mm*. Tracking experiments in that study also show sub-millimetric errors while tracking the ball during translations of 15 *cm* to 40 *cm*.

$$r = \frac{\sin b * d}{\sin a} \tag{II.1}$$

Some laser scanners also allow for the scalar encoding of range data. Typically laser scanners use an RGB laser (i.e. three different wavelengths coupled together) for both range data and color information. The color data is extracted per range point by using a diffraction prism on the receive end [43]. The laser scanner used for this thesis implements a different approach for scalar encoding. Scalar values were recorded as RGB data in a bitmap via CCD at the time of scanning.

Figure II.1: Laser scanner used to acquire textured point clouds.

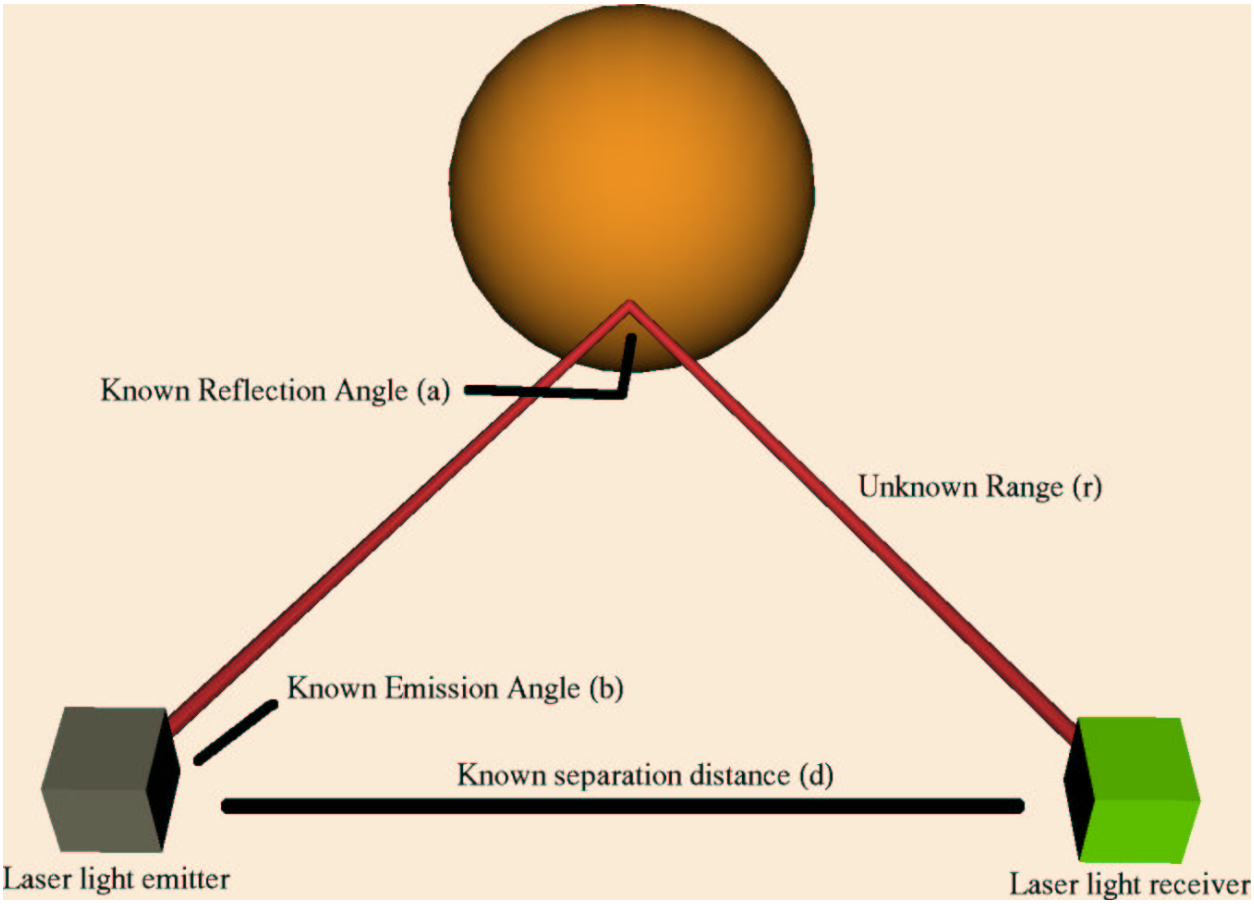

Figure II.2: Graphical Law of Sines

In this thesis the RGB data was converted into luminance (Y) values using a linear transformation (see Equation II.2).

$$Y = R * 0.299 + G * 0.587 + B * 0.114 \tag{II.2}$$

A single color channel was used in the registration process to reduce the complexity of the current algorithm. Scalar encoding of the point cloud was done via the texture map coordinates ($u, v \in [0,1]$) reported from the scanner. The registration between scanner coordinates and texture coordinates was calibrated at the manufacturer. Accuracy of the registration has not been verified, but is being planned as future research. In most graphics applications, the process of assigning to scalar values to the point clouds for visualization (texture mapping) occurs in hardware. However, for the purposes of this thesis, the texture mapping process was performed manually. The texture coordinates were scaled to the size of the captured bitmap[1], floored to the closest integral value and the resulting texture was recorded as VTK data attributes. Figure II.3 shows the process of generating textured point clouds from the data collected by the scanner. Manually texturing the point cloud reduced unnecessary computations during the registration process. For the point clouds from the laser scanner, the geometry was stored directly and the topology was defined as each point by itself. Dataset attributes for the point clouds included texture map coordinates and scalar values. For the bitmaps, a regularly spaced (structured) grid with scalar values representing the bitmap was used. A VTK source class (process object) was written to parse and read the binary data file from the scanner and output the point cloud and bitmap as two separate data outputs. A VTK filter class was used to generate luminance values from the RGB data bitmap. Finally, another VTK filter class was developed to manually texture the point cloud given the point cloud and bitmap as inputs.

To generate textured surfaces from MR volumes, a surface projection algorithm was used (Analyze AVW - Biomedical Imaging Resource). The MR volumes were gadolinium enhanced coronal slices of the brain (1.015625 *mm* resolution in the slice plane and 1.5 *mm* out of plane) that were segmented by hand to preserve the vessel structure. Rays were cast down the axial axis of the

[1] 640x480 pixels for the scanner used in this paper.

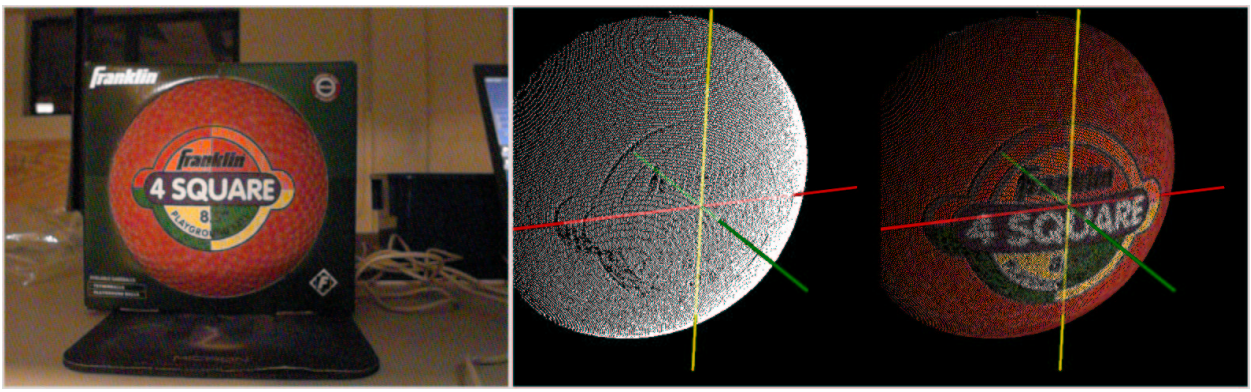

Figure II.3: Texture point cloud generation from the laser scanner. Left to Right: CCD Bitmap captured at the time of scanning, point cloud captured at the time of scanning, textured point cloud after texture mapping process.

volume. Only voxels with intensity values greater than five (out of 255) were recorded as surface points. The texture at a given point was calculated by averaging the first five voxels following the surface voxel (see Figure II.4). Finally, the surface was windowed empirically between 0 and 145 to provide high contrast between vasculature and tissue in the point cloud. The resulting dataset and its scalar attributes were used for registration purposes. A high resolution surface was created using bilinear interpolation (see Equation II.3 and Figure II.5) and super-sampling the surface in and out of the image plane. The surfaces used in this thesis were super-sampled 2x in the saggital axis and 4x in the coronal axis. The effect of super-sampling can be see in Figure II.6. The edge effects seen with increasing super-sampling and their influence on the registration is discussed in the results section.

$$I(x+r,y+q) = (1-r)(1-q) * I(x,y) + q(1-r) * I(x,y+1) + r(1-q) * I(x+1,y) + rq * I(x+1,y+1) \quad \text{(II.3)}$$

II.2 Surface Registration Using Mutual Information

The registration framework of this thesis, called SurfaceMI, involved two primary steps in its execution. The first step involved acquisition and preparation of the registration surfaces. The scanner

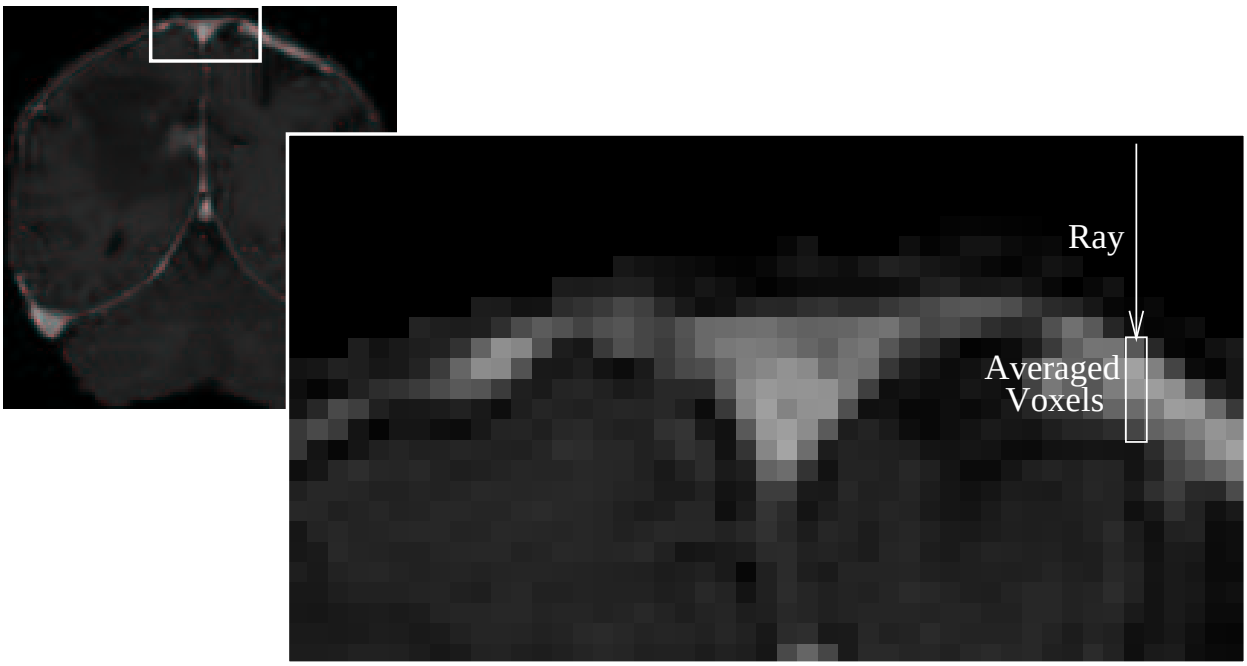

Figure II.4: Surface Projection Algorithm.

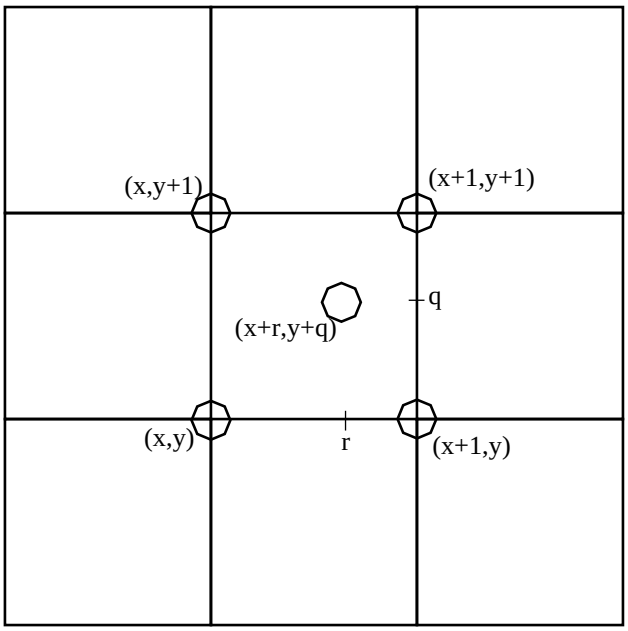

Figure II.5: Graphical Bilinear Interpolation.

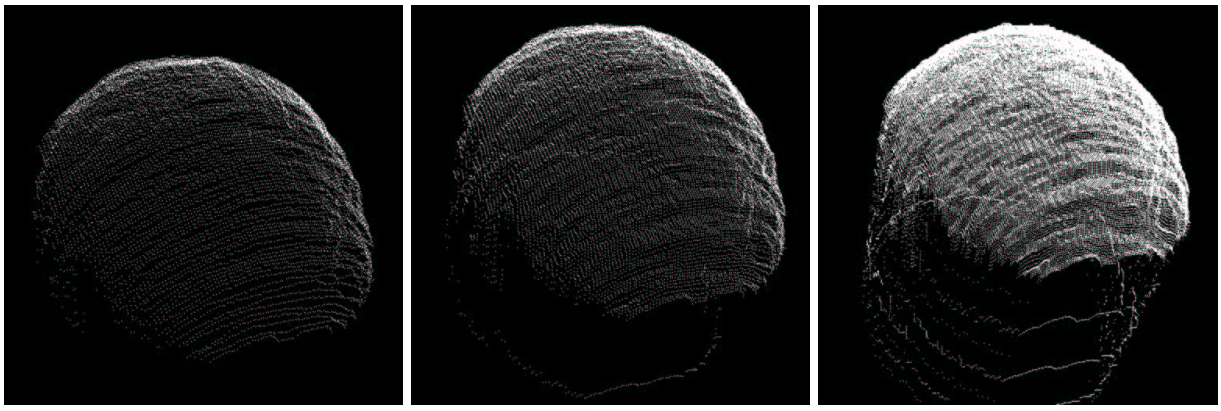

Figure II.6: Effect of bilinear interpolation on surface projection. From left to right: no interpolation, 2X interpolation in the coronal axis, 4X interpolation in the coronal axis and 2X interpolation in saggital axis.

was placed approximately 30-60 *cm* from the surface of interest using a tripod. The extents of the scanner's fan beam were established and the laser stripe was passed over the surface in approximately 5 seconds. Data collected via the scanner was post-processed off-line to remove features from the scan that were not used for registration. The MR surfaces were acquired according to the surface projection algorithm outlined earlier.

The final step in the approach was to perform surface registration using a two-stage process. To reiterate, the goal of the algorithm was to find T (a 4x4 matrix) such that the trace in Equation I.2 was minimized. In the first stage, an iterative closest point (ICP) algorithm was performed initially to align the point clouds of interest (i.e. laser-scanned surface and/or MR surface). The Procrustes transformation in each iteration of the ICP was calculated using an SVD method, outlined by Arun [33]. The SVD method utilizes cross-covariances between corresponding fiducials to reduced the trace of the registration. The algorithm is as follows for two sets of corresponding points (the source points, which are registered to the target points):

1. Calculate D_t, the distance of each target point to the centroid of the target points
2. Calculate D_f, the distance of each source point to the centroid of the source points
3. Calculate $H = D_t D_f^T$

4. Perform an SVD on H, resulting in U, D, and V matrices[2]

5. The rotation matrix R in T is given by UV^T

6. Finally the translation is given by calculating the difference in centroids

To implement the ICP algorithm, the SVD solution to the Procrustes problem was used iteratively (i.e. each rotation matrix calculated was concatenated to the previous matrix) until the mean closest distance fell below the resolution of the surface (empirically determined to be ≤ 0.1 *mm*).

The standard (exhaustive) search algorithm used to determine corresponding fiducials for the ICP was replaced with an optimized K-D search tree [44]. Proposed originally by Bentley, K-D trees are optimized binary search trees for multi(K)-dimensional spaces. The search tree was generated by partitioning the input dataset at each level along the median of the dimension with the greatest range. The tree was terminated when there are no more points to be partitioned at a given sub-tree. An example dataset and resulting K-D tree can be see in Figure II.7. Searching for nearest neighbors is done by traversing the the tree in a manner similar to standard binary trees. Given a query value, determine whether the value is less than, greater than, or equal to the value at any given sub-tree. The conditional was evaluated at the root node for every sub-tree for only the dimension being partitioned at that node. The search moves down the tree in the direction of the conditional that is satisfied. However, for K-D trees the size of the partitions in k-dimensional space must be tracked as the search progresses. Furthermore, when appropriate, traversing the complimentary branch for a given sub-tree must occur in order to find the *true* nearest neighbor. Optimized searching algorithms are outlined in [44][1][45]. The performance gained with K-D trees compensates for its complex implementation. For a search composed of N points in k dimensional space the search time goes from $O(N^2)$ in an exhaustive search to $O(N \log_k N)$ in a K-D tree search. This thesis used a C++ implementation of K-D tree creation and searching by David Mount called ANN [45]. ANN is extensible to any integral dimension k; this might be of benefit in future work, as the scanner returns 6 dimensional data by nature. Using the optimized nearest

[2] U and V are unitary matrices and D is a diagonal matrix containing the singular values of H, where $H = U^{-1}DV$

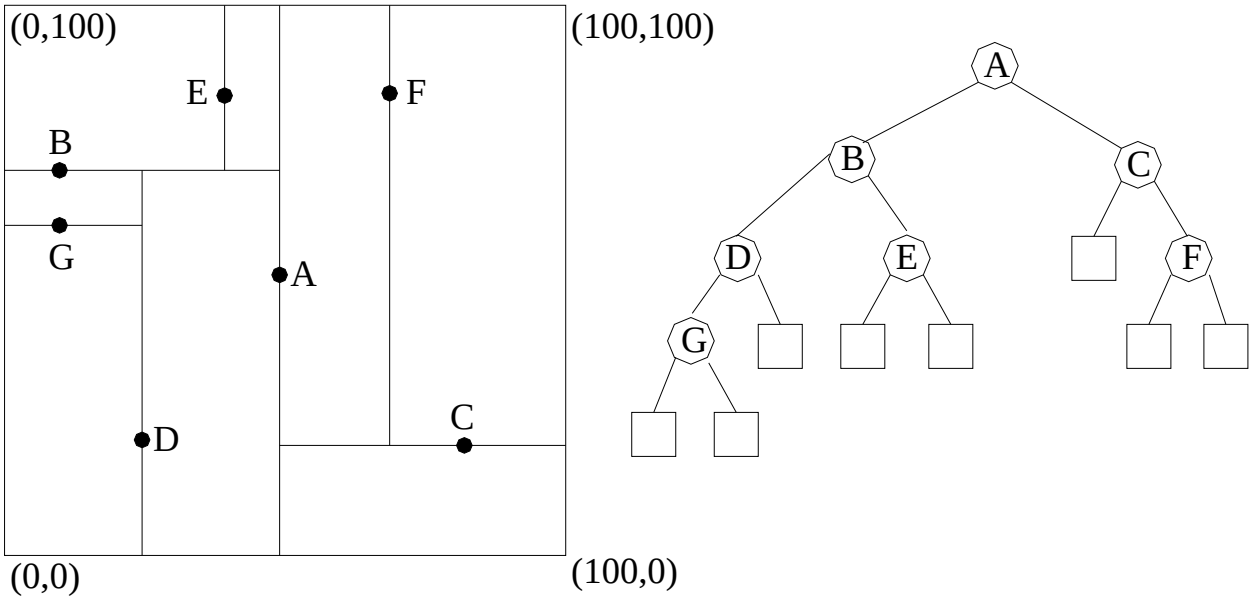

Figure II.7: An example K-D tree generated from Table II.1. Reproduced from Bentley [1].

Table II.1: Table of data used to generate the K-D Tree in Figure II.7.

Point	Location
A	(50,50)
B	(10,70)
C	(80,85)
D	(25,20)
E	(40,85)
F	(70,85)
G	(10,60)

neighbor search and the SVD implementation in VTK allowed accurate and efficient calculation of ICP transformations.

The ICP correspondence provides the necessary relationship to proceed with the second stage, a constrained intensity-based registration, provided by NMI. As reported earlier NMI is used to register random variables based on a mathematical information criteria. For the purposes of this thesis, the information criteria was calculated using histogram methods. The intensity at each point in a given surface cloud was binned between 0 and 255. Binning provides a quick and efficient way of approximating the probability density function (PDF) for the intensities in the cloud. Joint PDF's were calculated by associating intensities in two different clouds according to the nearest neighbors. Again, K-D trees were used to accomplish this task quickly. In order to penalize non-

overlapping surfaces, closest points that were not within the resolution of the surfaces were binned to a 0 intensity value in the joint pdf [3]. Marginal and joint Shannon entropies were calculated using non-zero bins in the respective histograms and (I.5). Finally, the calculated value of NMI (I.6) was passed into the optimization pipeline.

The optimization chosen for this was Powell's method taken from [46]. Powell's optimization is a direction set method for optimization in multi-dimensions. The optimization determines conjugate directions for line minimizations at each iteration. Conjugate directions implies "non-interfering" lines for optimization. That is, optimizing in any one of the directions will not compromise the optimization in any other direction. An efficient method for determining conjugate directions is to use the first derivatives of the objective function (called "Conjugate Gradient Descent" optimization). Ideally, for this method to work, functional forms of the objective and its derivatives must be known. In some cases, if the functional forms are not known, numerical approximations can be substituted. Experiences during the development of the registration algorithm proved that numerical approximations of the derivatives could not be employed in the optimization. Local minima in the objective functions space and the shape of the space itself prohibited gradient descent methods from converging to the global minimum. Although the shape of the objective space has not been characterized, empirical evidence indicates that it is ellipsoidal with a high major axis to minor axis ratio. Thus, the gradient in the direction of one of the basis vectors might be orders of magnitude larger than the other gradients. This property of the space easily confounds direct gradient descent methods, as one direction dominates the optimization process. Furthermore, using numerical approximations for the derivatives does not provide truly conjugate directions for optimization. Thus, the conjugate methods of optimization succumb to local minima. Powell's method of optimization compensates for the shape of the objective space by calculating a better approximation to the conjugate directions for line minimization at each iteration. After the conjugate directions were found in Powell's method, a line minimization was done in each direction. The line minimization was done using Brent's method of inverse parabolic interpolation,

[3]The criteria for overlap was that the closest point must be less than 1 millimeter

which is quadratically convergent. For a bracketed minimum, the minimum was found by fitting a parabola through three points within the bracket. The objective function was then evaluated and re-bracketed at the minimum of the fitted parabola. This process was repeated until the minimum was found for the given direction, and was repeated for each conjugate direction.

To further help the optimization process, a geometry constraint was imposed on the calculated transformation. The constraint requires the alignment transformation to operate in spherical coordinates with a fixed radius. This constraint was hypothesized based on empirical observations of the surface of the brain. To implement the constraint, a sphere was fitted geometrically in a least-squares sense to the target surface [47]. Given the set of points X, the fitting was provided by minimizing the objective function in Equation (II.4).

$$\min\left(\sigma^2\right) = \min\left(\left(X - F(\vec{a})\right)^T \left(X - F(\vec{a})\right)\right) \tag{II.4}$$

where $F(\vec{a})$ is the parametric equation of a sphere. The parameters $\vec{a}$ are found using Gauss-Newton iteration method:

$$\vec{a}_{k+1} = \vec{a}_k + \lambda\Delta\vec{a} \tag{II.5}$$

with λ step-size. $\Delta\vec{a}$ is found using an SVD decomposition of the Jacobian matrix:

$$J_k = \frac{\partial F}{\partial \vec{a}_k} = UDV^T \tag{II.6}$$

where U, D, and V^T are the result of the SVD (described earlier), leading to,

$$\Delta\vec{a} = VDU^T \times \left(X - F(\vec{a}_k)\right) \tag{II.7}$$

The iterations were stopped when $\Delta\vec{a}$ was below a threshold value of 0.01. For a complete description of the fitting process refer to Ahn [47].

Given the radius of the fitted sphere, all transformations of the source surface were constrained to move along the surface of the sphere. By enforcing this restriction on the transformation, the

degrees of geometric freedom were reduced from six to three, i.e. elevation ϕ, azimuthal θ, and roll ψ at the fitted radius r.

CHAPTER III

EXPERIMENTS

A series of experiments were developed to gauge the limits of the algorithm. Additionally, these initial trials also gauged the computational costs of the algorithm. The first series of experiments tested the accuracy of the algorithm under intra-modal conditions. Having successfully developed the algorithm using the first series of experiments, the second series experiments tested the registration algorithm under simulated multi-modal conditions. Results to both series of experiments are discussed in the results section.

A series of intra-modal experiments were used to verify the accuracy and robustness of the newly devised surface registration algorithm. The first intra-modal experiment in this series was to register two surfaces of a ball (Franklin Sports INC., Stoughton, MA, 02072) from the range scanner. The ball was used to simulate the hemispherical geometry of the exposed brain surface seen intra-surgically. The surfaces used in this paper for registration experiments occupied a solid angle of $\Omega = 1.2\pi$ steradians[1] and contained 67257 points (see Figure III.1). A known spherical transformation about the fitted radius was applied to the target surface to generate the floating surface. The limits for the elevation and azimuthal angles were sampled were between ± 13 degrees and the roll angle was sampled between ± 25 degrees. Five hundred uniformly distributed combinations of ϕ, θ, and ψ were tested for registration accuracy.

Having tested the intra-modal registration accuracy of the laser range scan data, a second set of experiments tested registration accuracy of the point clouds generated from the surface projections of the MR volume. The target surface generated via surface projection and clipping had a solid angle of approximately $\Omega = .38533\pi$ steradians and contained 48429 points (see Figure III.2 and III.3). The misregistration protocol from the ball experiments was applied to the brain surface. The range for the parameters ϕ, θ, and ψ were the same as those for the ball but the transformation was applied about the fitted center and radius of the brain. Again, the parameters for the known

[1]The solid angle of a unit sphere $\Omega = 4\pi$ steradians.

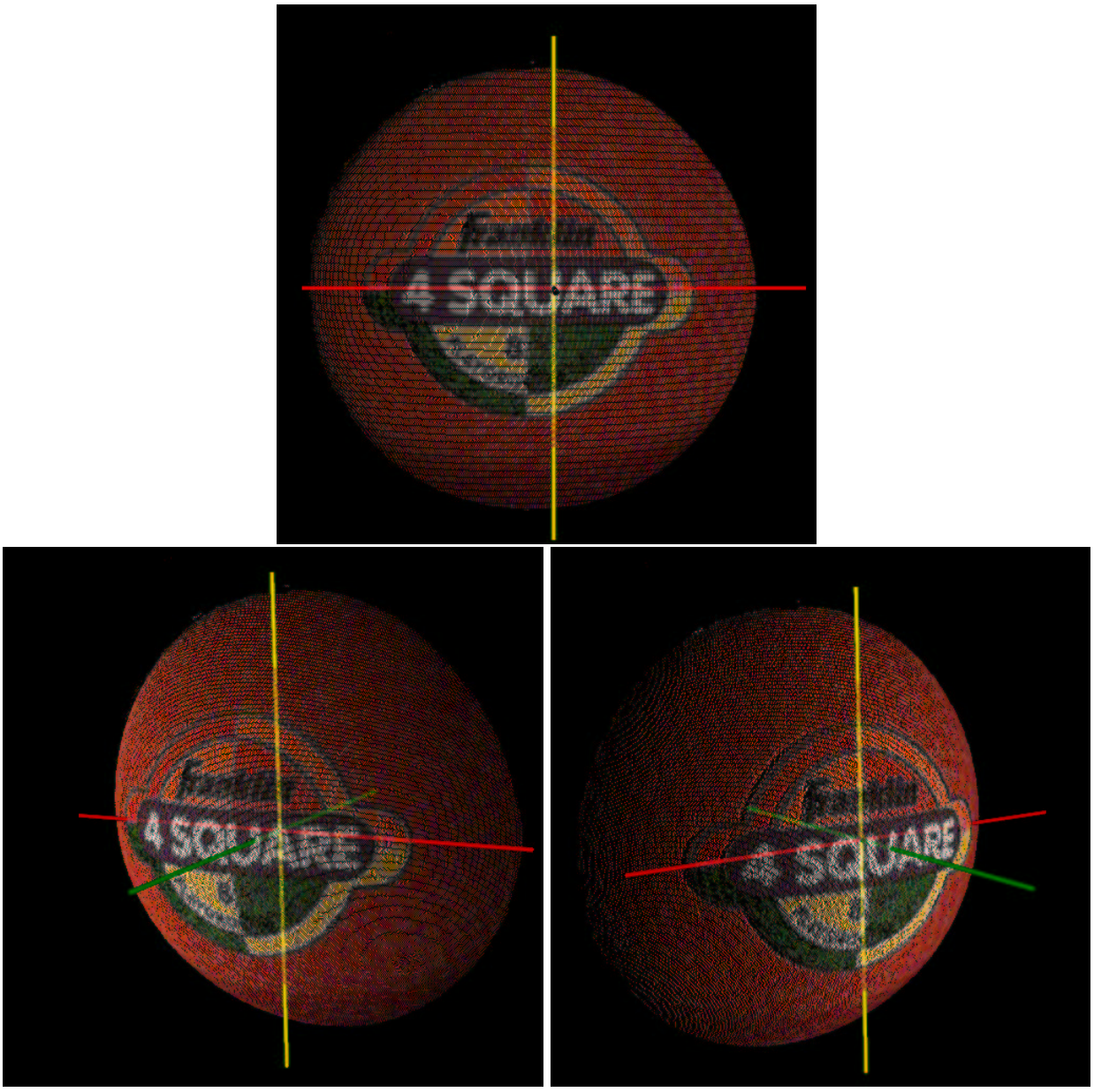

Figure III.1: Sample textured point cloud generated using a laser range scanner.

transformations were sampled for 500 trials.

The third set of experiments outlines the efficacy of the developed algorithm in registering surfaces across modalities. Inter-modality surfaces were simulated by inverting the texture of the point cloud generated via surface projection. Texture values were inverted according to the following equation,

$$I'(x,y,z) = 255 - I(x,y,z) \tag{III.1}$$

Five hundred trials were run using the target surface defined earlier and different ROIs from the inverted surface projection as the floating surfaces. The ROIs were generated by varying the normal of the clipping plane used to create the target surface between ± 0.1 *cm* in the sagittal and coronal axis while holding the axial value at 1 *cm*. To create the misregistration between the float and target surface, each surface was re-centered about it's geometric centroid. An initial approximation to the correct registration was provided by applying an ICP transformation to the floating surface.

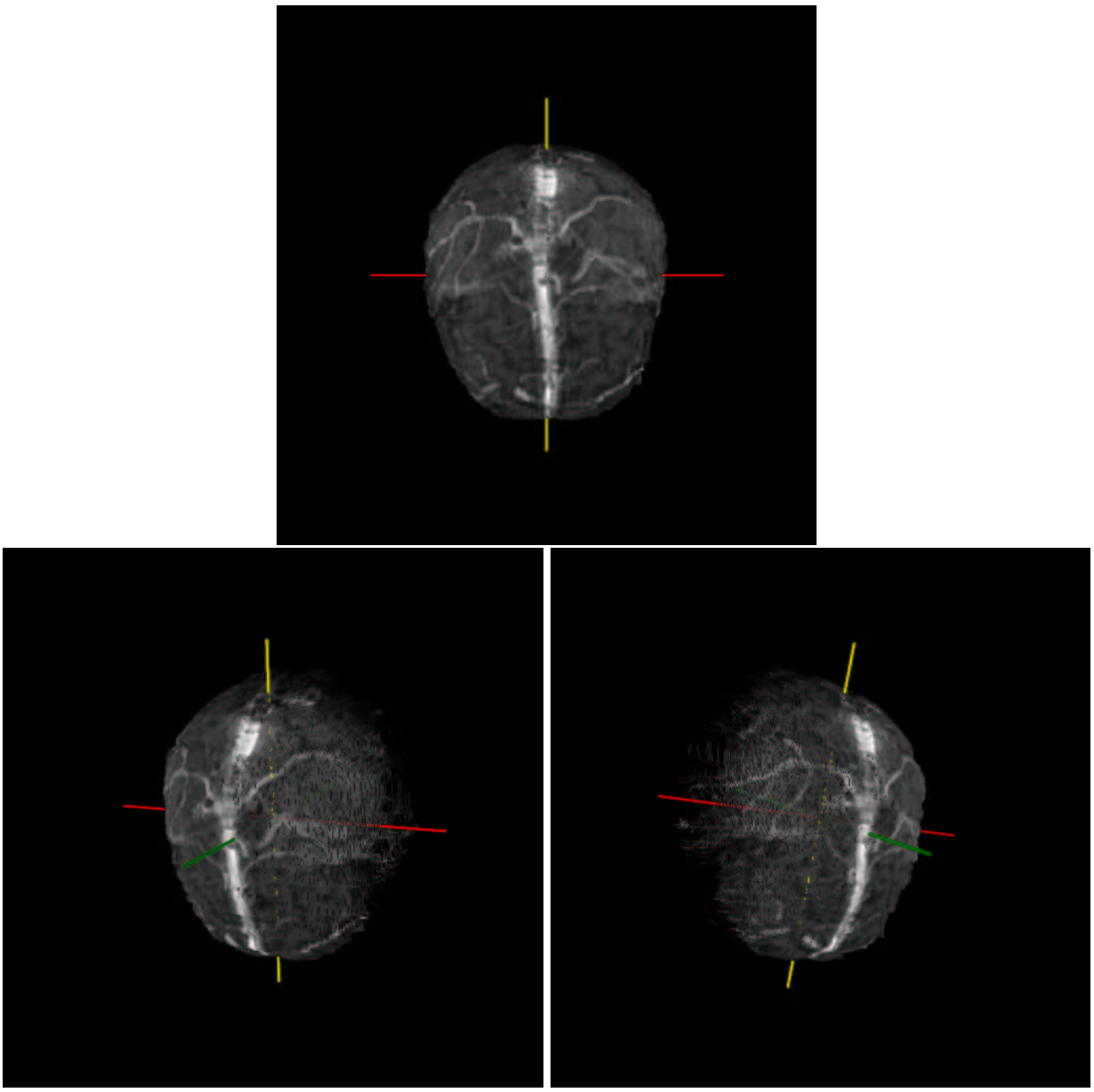

Figure III.2: Sample textured point cloud generated using surface projection on a Gadolinium enhanced MR volume.

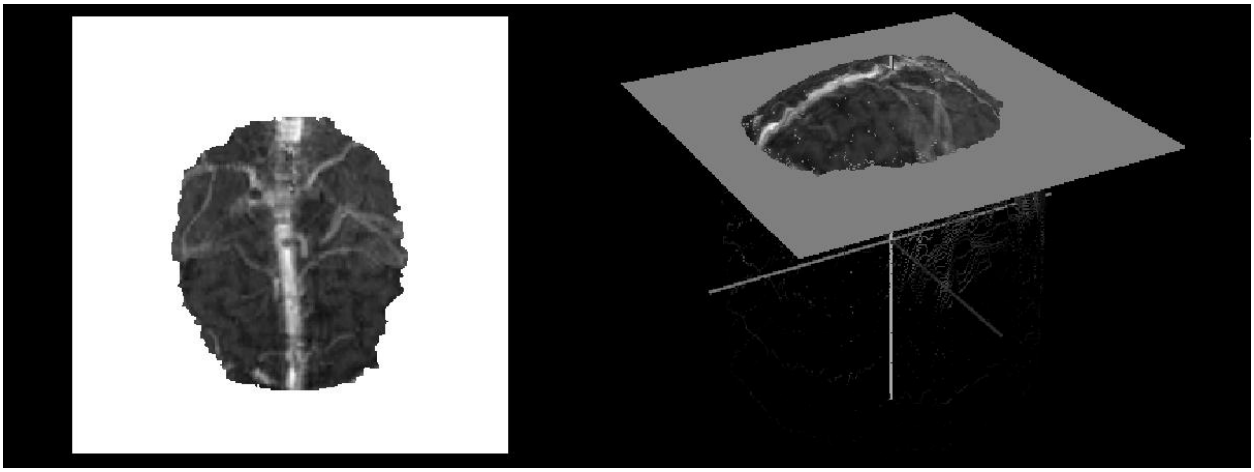

Figure III.3: Use of a clipping plane to select a region of interest in the surface projection.

CHAPTER IV

RESULTS

Since the same scan was used for both target and floating surfaces in the registration experiments, the one-to-one correspondence in points was known. This allowed calculation of the root-mean-squared target registration error (RMS TRE), as defined by Fitzpatrick and Mandava [48], between point clouds after registration. The equation for RMS TRE (given in IV.1) is as follows,

$$RMS\ TRE = \sqrt{\left(\frac{1}{N}\sum_{j}^{N}\left(y_j - T(x_j)\right)^2\right)} \tag{IV.1}$$

where y_j is a point on the target cloud and $T(x_j)$ is the corresponding point on the floating cloud transformed in the coordinate space of the target cloud. The one-to-one correspondence also meant that the NMI for a fully optimized registration was known. Thus, the registration results from the 500 trials are split into two categories. The first set, over the entire 500 trials, yielded an RMS TRE of 11.38 ± 28.75 *mm*. The second category represents the 345 trials where the registration attained an ideal value for NMI, i.e. the maximum value for NMI given a set of marginal entropies[1]. In the successful registration set the RMS TRE was 0.20 ± 0.05 *mm*. There was no significant difference between the means for ϕ, θ, and ψ, between the two categories. This result implies that the range for successful registration is within the sampling range of ϕ, θ, and ψ. An indication of the robustness of the algorithm is the 70% of registration trials that registered to better than 1 millimeter accuracy. Furthermore, the RMS TRE results of the experiment on the ball show that SurfaceMI and Powell's optimization register the surfaces very accurately (i.e. below the tolerances of the scanner) when successful. A sample result of the registration algorithm on the ball can be seen in Figure IV.1. Note that the sampling range used in this paper is anticipated to be much greater than what will be observed during surgery. Inter-operatively, the expected range of misregistration should be

[1] In this case, since both marginal entropies are the same and the joint probability of a correctly aligned surface is equal to the marginal entropy, the ideal value of NMI is $|2|$.

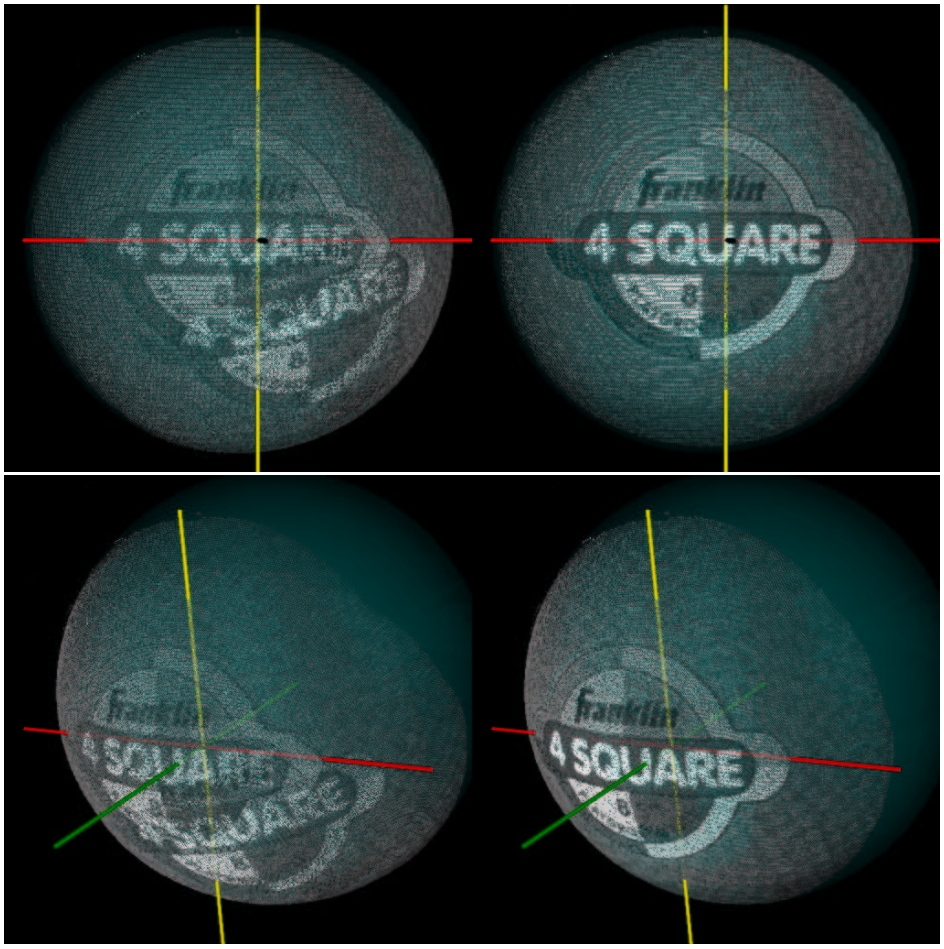

Figure IV.1: Sample registration results for the ball phantom with spherical constraint. Top row, from left to right: two misregistered surfaces, two surfaces after registration. Bottom row, left to right: off-axis view of misregistered surfaces, off-axis view of registered surfaces. Initial misregistration of 15 degrees in ϕ, θ, and ψ

.

no greater than ± 5 degrees in each parameter (in this range the ball phantom results are 100% successful).

All trials using the intra-modal imaging phantom resulted in an ideal value of NMI. The RMS TRE for these trials were 0.14 ± 0.04 *mm*. The difference in the results of the brain and the ball are likely due to the differences in the topologic distribution of the intensity information. Most of the intensity information of the ball is contained in the central area of the surface. In some cases, when the initial mis-registration of the ball causes sufficient non-overlap of the central area, the algorithm can not register the surfaces correctly. For the brain, the intensity pattern of the vessel structure occupies most of the surface. Thus, even though the brain's surface occupies a smaller solid angle than that of the ball, the distribution of the intensity pattern allows for more severe misregistration to be aligned. A sample result of the registration results on the brain surface can be seen in Figure IV.2.

In the simulated inter-modal registration experiments, statistical analysis of the results show that SurfaceMI did produced a more accurate registration of the surfaces over all trials (t-test: $p \leq 0.05$). The second category in Table IV.1 shows descriptive statistics for trials in which the RMS TRE of the registration was less than 2 standard deviations plus the mean RMS TRE calculated earlier using known transformations. There were only 137 trials which registered the target and floating surfaces to this tolerance. The variance of the successfully registered trials is significantly different from the entire trial population. The extent of the variance is reduced by an order of magnitude for the successful registrations. Analysis of the surfaces that failed to register showed that the spherical constraint prevented accurate surface registration. In general, the algorithm failed to register surfaces clipped from or containing the periphery of the surface projection. The periphery of the surface projection contained a much higher surface curvature when compared to the target surface. This discrepancy in surface curvatures between target and floating surfaces caused the sub-optimal registrations. For cortical resection and retraction, the visible surface of the brain will likely be from a single region, this inherent region constraint will be incorporated into future iterations of the algorithm. A sample of the simulated inter-modality registration experiment can

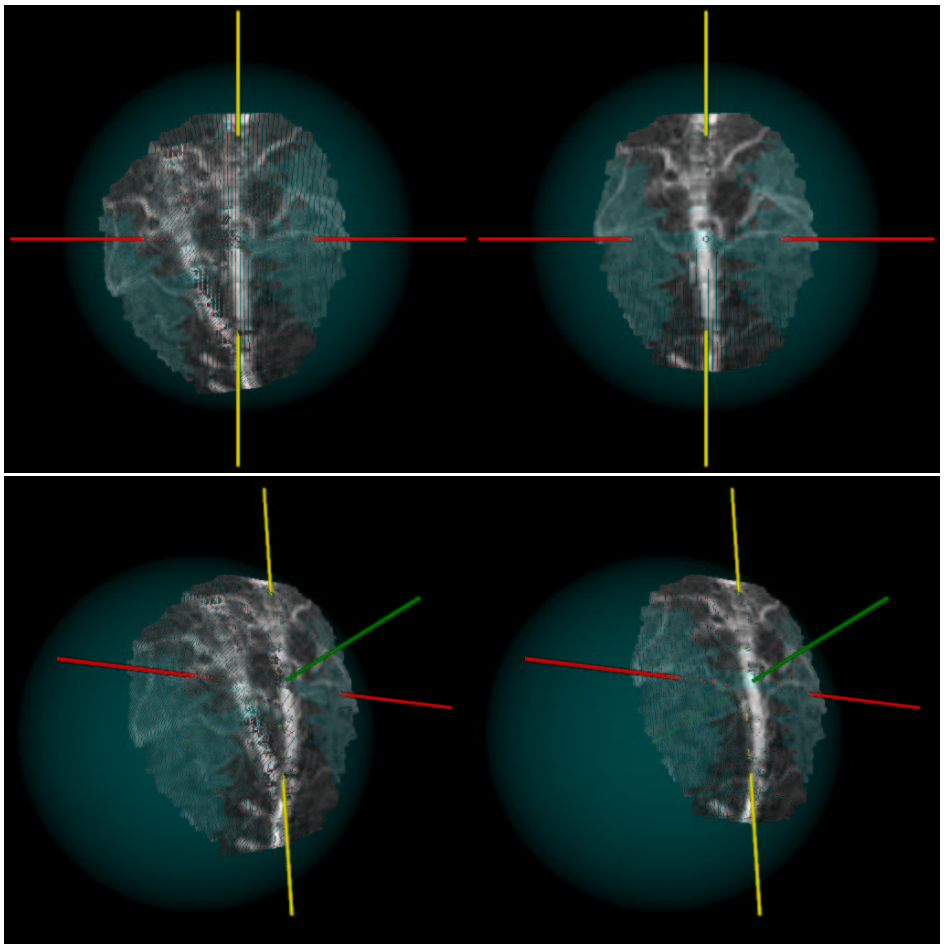

Figure IV.2: Sample Registration Results for the brain phantom with spherical constraint. Top row, left to right: two misregistered surfaces, two surfaces after registration. Bottom row, left to right: off-axis view of misregistered surfaces, off-axis view of registered surfaces. Initial misregistration of -15 degrees in ϕ, θ, and ψ.

Table IV.1: Results for simulated inter-modal registration of the brain phantom using Surface MI.

	All Trials	Successful Registration Trials
Number of Trials	500	137
ICP RMS TRE (mm)	5.25 ± 3.50	2.69 ± 1.81
MI RMS TRE (mm)	3.36 ± 7.17	0.21 ± 0.06

be seen in Figure IV.3. The results are shown with an intra-modal registration of the same surfaces for clarity.

Figure IV.4 shows the results of each set of experiments in histogram fashion. As the figure shows, the results for both intra-modality experiments show high success rates for TRE's under 0.5 millimeter. The results in the intra-modal brain experiments showed a lower percentage below 0.5 millimeter and, but also a a larger percentage between 0.5 and 3.5 millimeters when compared to the intra-modal experiments. The results depicted in the histogram supplement the conclusions drawn from analyzing the RMS TRE's within each set of experiments. That is, the concentrated intensity pattern in the sphere phantom prevented proper alignment. However, the distribution of the sphere phantom correlated well with the brain phantom, in that the successful and non-successful registrations were mutually exclusive with regard to TRE. Thus, in very few occasions when the registration failed did it produce RMS TRE below 3.5 *mm*. The inter-modality distribution shows that there were more instances, as compared to the intra-modal trials, where the algorithm did not reach ideal NMI, but still produced RMS TRE values below 3.5 *mm*. This is in contrast to the intra-modal trials and shows that even when the algorithm fails to reach a highly accurate alignment it may achieve a "good" ($\leq 3.5mm$) alignment.

The results here have shown that SurfaceMI registers textured surfaces well. The topological distribution of the texture effects the ability for SurfaceMI to register. However, good topographical texture distributions are expected intra-operatively. Intra-modal registrations demonstrate low error residuals when successfully registered, but generated very high residuals when unsuccessful. Simulated inter-modal registrations exhibited lower residuals for unsuccessful registrations, implying that SurfaceMI can register reasonably well even when unsuccessful.

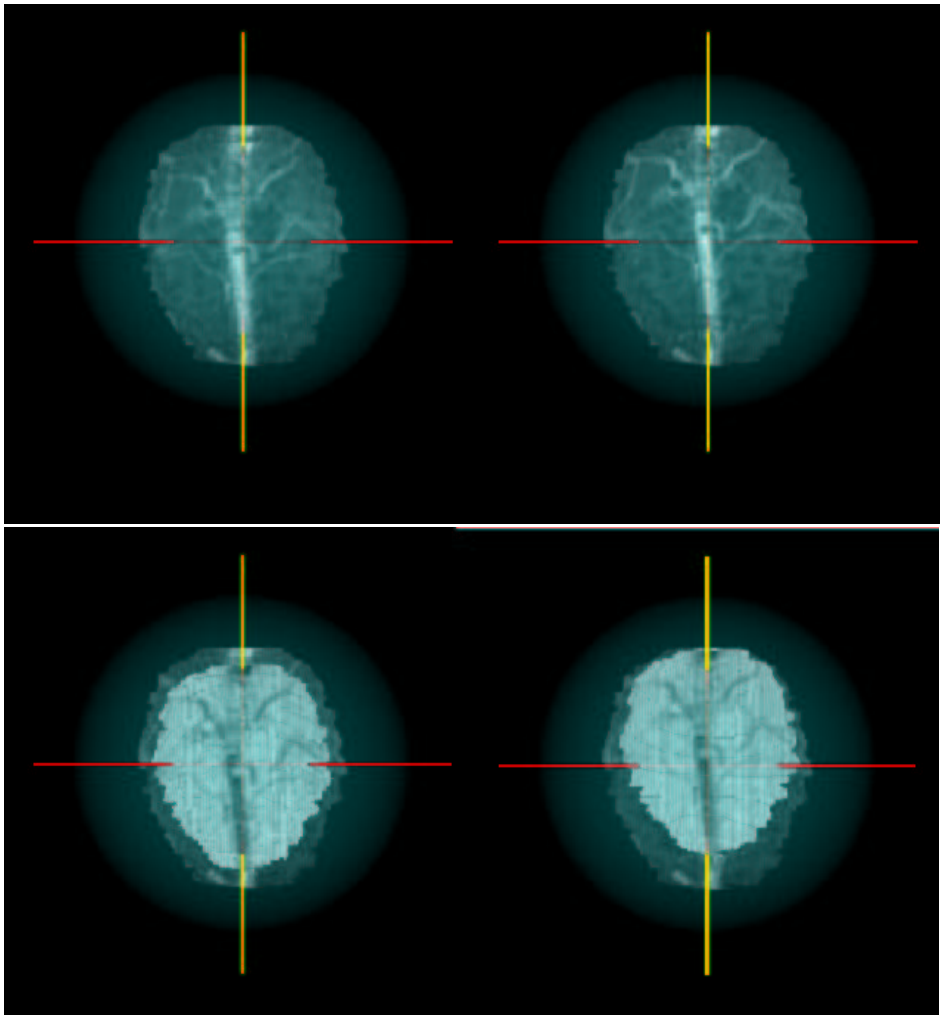

Figure IV.3: Sample Registration results for simulated multi-modality registrations of the brain phantom. Top row, from left to right: two intra-modal surfaces registered via ICP and after registration via SurfaceMI. Bottom row, from left to right: two simulated multi-modal surfaces registered via ICP and registered via SurfaceMI. Clipping plane parameters: saggital = 0.02 *cm*, coronal = 0.1 *cm*, and axial = 1 *cm*.

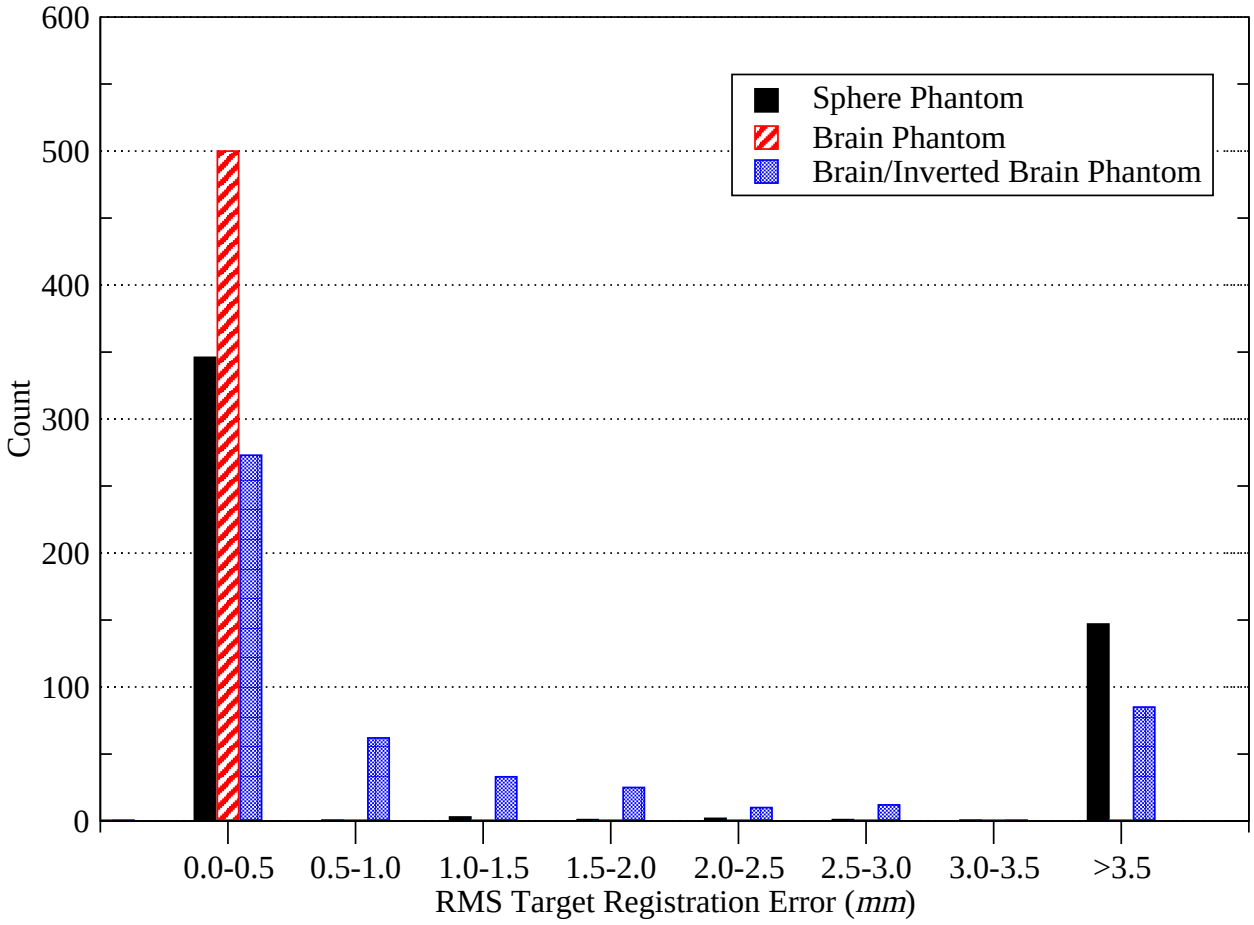

Figure IV.4: Distribution of target registration errors for each set of experiments.

CHAPTER V

CONCLUSIONS

The results of this thesis show that the ICP and MI framework is a useful tool for cortical surface registration. Results of both intra- and inter-modality surface registration show sub-millimetric accuracies using a phantom. This thesis outlines preliminary steps taken with the laser range scanner and the algorithm. Future work, to be discussed in the following chapter, will hopefully prove the value of both the laser range scanner and unique surface registration algorithm in model-updated image guided-surgery.

The use of a laser range scanner in the operating room is a novel method of intra-surgical surface characterization. As seen in Figure VI.1, this method has been shown to be a viable non-contact method of capturing intra-operative data. The surfaces collected by the scanner are accurate with regard to the physical world and provide, not only geometric data, but also rich surface texture information. The wealth of information contained within the scans will provide critical information for computationally updated IGP.

With respect to incorporating the feature-rich laser range scan data, a novel registration algorithm has been developed. The algorithm, which is built on a framework sensitive to intensity information (i.e. mutual information), capitalizes on both the intensity and geometry contained in each scan. To provide data similar to that acquired by the laser range scanner, a method to extract textured point clouds from the pre-operative data has been developed. The surface extraction method has shown that gadolinium enhanced MR images provide good texture and geometry information for the registration algorithm.

The results of the techniques discussed in the thesis show viability for clinical application. The intra-modality experiments demonstrate the successful modification and application of existing registration techniques to the specific problem of registering textured point clouds. The simulated inter-modal experiments show that the algorithm can effectively extended to multi-modal datasets, i.e. a patient-specific range scan to his or her pre-operative image volume.

The import of the ideas and methods outlined in this thesis are a critical component in the development of model-updated IGP. Registering intra-operative data to pre-operative data will allow for boundary conditions in the computational models used for model-updated IGP. The computational models will then provide the physician with intra-surgically relevant images which can be used for more accurate therapy delivery.

CHAPTER VI

FUTURE WORK

There are many research avenues to pursue as a result of the work presented in this thesis. The immediate goal of future work is to verify *in vivo* accuracy of the registration algorithm. Preliminary designs for true inter-modal registration experiments include using watermelons with CT/MR contrast-enhanced vasculature inlaid on the surface. The vasculature will be imaged using the scanner as well as CT and MR imaging devices. The methods described in this thesis will then be applied for registration. Error residuals similar to those reported in this thesis will be reported for the inter-modal registrations. These phantoms will also be validated using a gold standard for registration that is being developed by Cash et al. Furthermore, the phantoms will allow for comparisons with existing registration techniques, e.g. Nakajima's method for point based registrations using vessel bifurcations and ICP methods using extracted vessel contours. These experiments will examine the potential registration accuracy in an inter-modal setting using the laser range scan data.

In vivo proof of concept and accuracy studies are currently under way. In these studies, consenting patients primarily under going tumor resection and similar surgeries will be monitored during the course of therapy. These patients will be operated on using image-guidance with the scanner also being tracked by the image-guidance system. Before the skull cap is removed, exposing the area of therapy, a laser scan will be taken. Another scan will be taken after removal of the dura. Subsequent scans will be taken periodically during the course of surgery. This experimental setup will map the laser range scanner space to physical-space, and consequently image-space. This mapping will allow for the registration results using the scanner to be checked against results provided by the image-guidance system. Furthermore, this experimental protocol will test the ability to of the scanner to track the intra-operative deformations. After surgery, all of the scans will be registered and verified for accuracy. An example dataset from surgery is given in Figure VI.1. This dataset clearly shows that the cortical surface can be resolved with the current laser scanner

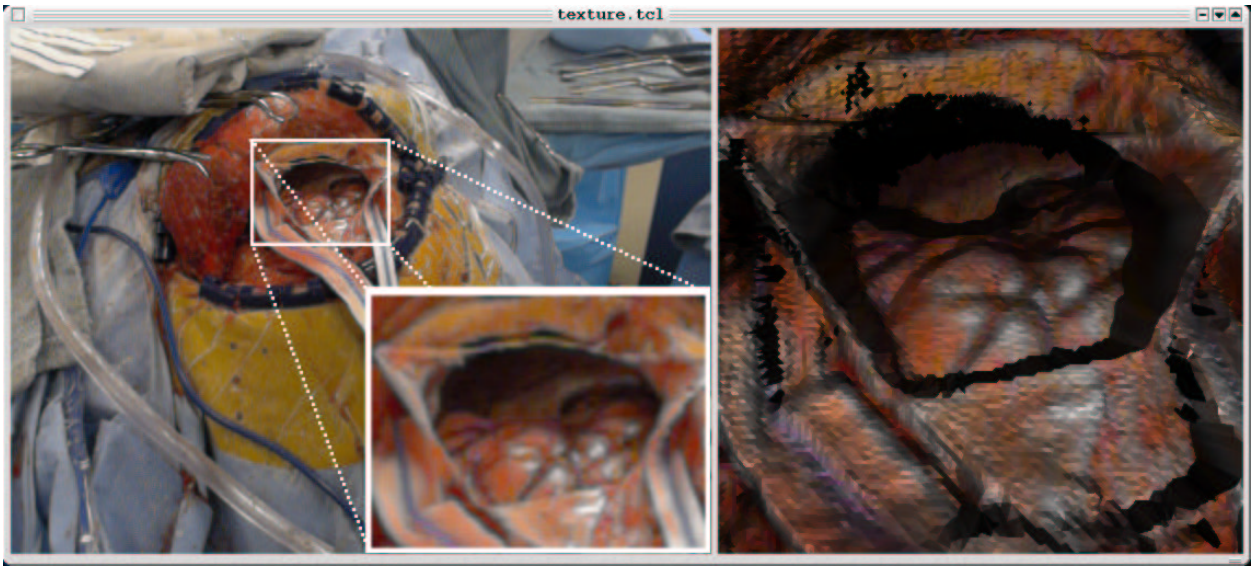

Figure VI.1: Example dataset taken with the laser range scanner in the operating room. Left, a CCD image of the surgical area. Right, a tessellated point cloud with texture mapped points on the right.

and thus can be used for *in vivo* validation.

The algorithm itself is also under research. Future iterations of the algorithm will use non-canonical basis sets for registration. Basis sets, like B-spline sets or Fourier sets will be used to allow for non-affine transformations from physical to image space. Arun's solution to the Procrustes' problem does allow for higher dimensions in the basis sets for registration. More pliant shape constraints on the registration algorithm are also planned for review. The ultimate goal would include finding a general form for the registration algorithm (that is computationally tractable) for any two surfaces over any number of degrees of freedom.

With regard to Mutual Information, different estimations of mathematical entropy are under investigation. Viola and Well's original work presented a method for probability density estimation called the Parzen Window [36]. This method uses a moving average of Gaussian distributions provided by the random variable [49]. Although this method is not anticipated to be less computationally intensive, it will allow for calculation of NMI in higher dimensions more easily. That is,

future NMI calculations might look like the following:

$$NMI = \frac{H(rx, gx, bx) + H(ry, gy, by)}{H(rx, gx, bx, ry, gy, by)} \tag{VI.1}$$

Also, the use of non-standard entropy measures, e.g. Renyi and Kullback entropies, is also under investigation [50][51]. The objective function space associated with these non-standard entropy measure might yield more tractable optimizations.

Another area of active research is more effective optimization of the Mutual Information criteria. The simple line set method used in this thesis will be replaced with more advanced meta-heuristic search strategies. One method under investigation is the Tabu search [52]. This search strategy allows one to use more simple search methods in a heuristic fashion. For example, in the specific case of optimizing the NMI in two textured point clouds, the Tabu search will use Powell's method for line minimizations within the search space. The Tabu search will then guide the optimization within the search space by expanding search areas out of regions of local minima, e.g. using Tabu criteria [52]. Initial experiences with this advanced search strategy show it to be an effective alternative to a purely numerical optimization.

Finally, this thesis and the work included are stepping stones in the path to accurate model-updated image guided surgery. Novel work has to be completed in the area of the physical model, the update procedure, and the image-guidance system for the complete model-updating application to be successful. These topics are to be looked at in the future as a part the development of model-updated image guided procedures.

REFERENCES

[1] J. L. Bentley. Multidimensional binary search trees used for associative searching. *Communications of the ACM*, 19, 1979.

[2] Robert L. Galloway. Personal correspondence, January 2002. Vanderbilt University Biomedical Engineering Graduate Student Research Day.

[3] R. L. Galloway. The process and development of image-guided procedures. *Annual Review of Biomedical Engineering*, 3:83–108, 2001.

[4] V. Horsley and R. H. Clarke. The structure and function of the cerebellum examined by a new method. *Brain*, 31:45–124, 1908.

[5] R. L. Galloway and Robert J. Maciunas. Stereotactic neurosurgery. *Critical Reviews in Biomedical Engineering*, 18(3):207–233, 1990.

[6] R. L. Galloway. The process and development of image-guided procedures. *Annual Review of Biomedical Engineering*, 3:83–108, 2001.

[7] C. R. Maurer, J. M. Fitzpatrick, M. Y. Wang, R. L. Galloway, R. J. Maciunas, and G. S. Allen. Registration of head volume images using implantable fiducial markers. *Ieee Transactions on Medical Imaging*, 16(4):447–462, 1997.

[8] Peter H. Schoenmann. A generalized solution of the orthogonal procrustes problem. *Psychometrika*, 31:1–10, 1966.

[9] J. B. West, J. M. Fitzpatrick, S. A. Toms, C. R. Maurer, and R. J. Maciunas. Fiducial point placement and the accuracy of point-based, rigid body registration. *Neurosurgery*, 48(4):810–816, 2001. English Article APR NEUROSURGERY.

[10] D. L. G. Hill, C. R. Maurer, R. J. Maciunas, J. A. Barwise, J. M. Fitzpatrick, and M. Y. Wang. Measurement of intraoperative brain surface deformation under a craniotomy. *Neurosurgery*, 43(3):514–526, 1998.

[11] C. Nimsky, O. Ganslandt, S. Cerny, P. Hastreiter, G. Greiner, and R. Fahlbusch. Quantification of, visualization of, and compensation for brain shift using intraoperative magnetic resonance imaging. *Neurosurgery*, 47(5), 2000.

[12] P. J. Kelly. Computer-assisted stereotaxic laser resection of intraaxial brain neoplasms. *Neurosurgery*, 64(3):427–439, 1986.

[13] Michael I. Miga, Keith D. Paulsen, F. E. Kennedy, V. M. Tronier, D. W. Roberts, A. Hartov, L. A. Platenik, and K. E. Lunn. Model-updated image-guided neurosurgery: preliminary analysis using intraoperative mr. *LNCS: Medical Image Computing and Computer-Assisted Intervention*, 1935:115–124, 2000.

[14] A. Nabavi, P. M. Black, D. T. Gering, C. F. Westin, V. Mehta, R. S. Pergolizzi, M. Ferrant, S. K. Warfield, N. Hata, R. B. Schwartz, W. M. Wells, R. Kikinis, and F. A. Jolesz. Serial intraoperative magnetic resonance imaging of brain shift. *Neurosurgery*, 48(4):787–797, 2001.

[15] L. D. Lunsford. Magnetic resonance imaging stereotactic thalamotomy: report of a case with comparison to computed tomography. *Neurosurgery*, 23(3):363–7., 1988.

[16] R. D. Bucholz, D. D. Yeh, J. Trobaugh, L. L. McDurmont, C. D. Sturm, C. Baumann, J. M. Henderson, A. Levy, and P. Kessman. The correction of stereotactic inaccuracy caused by brain shift using an intraoperative ultrasound device. In *Cvrmed-Mrcas'97*, volume 1205 of *LECTURE NOTES IN COMPUTER SCIENCE*, pages 459–466. 1997.

[17] C. Nimsky, O. Ganslandt, P. Hastreiter, and R. Fahlbusch. Intraoperative compensation for brain shift. *Neurosurgery*, 56(6):357–364, 2001.

[18] D. W. Roberts, M. I. Miga, A. Hartov, S. Eisner, J. M. Lemery, F. E. Kennedy, and K. D. Paulsen. Intraoperatively updated neuroimaging using brain modeling and sparse data, 1999.

[19] M. I. Miga, D. W. Roberts, F. E. Kennedy, L. A. Platenik, A. Hartov, K. E. Lunn, and K. D. Paulsen. Modeling of retraction and resection for intraoperative updating of images. *Neurosurgery*, 49(1):75–84, 2001.

[20] E. Fontenla, C. A. Pelizzari, J. C. Roeske, and G. T. Y. Chen. Using serial imaging data to model variabilities in organ position and shape during radiotherapy. *Physics in Medicine and Biology*, 46(9):2317–2336, 2001.

[21] C. R. Maurer, R. P. Gaston, D. L. G. Hill, M. J. Gleeson, M. G. Taylor, M. R. Fenlon, P. J. Edwards, and D. J. Hawkes. Acoustick: A tracked a-mode ultrasonography system for registration in image-guided surgery. *LNCS: Medical Image Computing and Computer-Assisted Intervention*, 1679:953–962, 1999.

[22] A. J. Herline, J. L. Herring, J. D. Stefansic, W. C. Chapman, R. L. Galloway, and B. M. Dawant. Surface registration for use in interactive image-guided liver surgery. *LNCS: Med. Image Computing and Computer-Assisted Intervention*, 1697:892–899, 1999.

[23] A. Herline, J. D. Stefansic, J. Debelak, R. L. Galloway, and W. C. Chapman. Technical advances toward interactive image-guided laparoscopic surgery. *Surgical Endoscopy-Ultrasound and Interventional Techniques*, 14(7):675–679, 2000.

[24] N. Hata, T. Dohi, H. Iseki, and K. Takakura. Development of a frameless and armless stereotactic neuronavigation system with ultrasonographic registration. *Neurosurgery*, 41(3):608–613, 1997.

[25] W. C. Lin and et al. Brain tumor demarcation using optical cpectroscopy; an *in vitro* study. *Journal of Biomedical Optics*, 5(2):214–220, 2000.

[26] W. C. Lin and et al. *In vivo* brain tumor demarcation using optical spectroscopy. *Journal of Biomedical Optics*, 73(4):396–402, 2001.

[27] Steven L. Hartmann. *Intraoperative identification and display of cortical brain function*. PhD thesis, Vanderbilt University, 2002.

[28] James D. Foley, Andries van Dam, Steven K. Feiner, and John F. Hughes. *Computer Graphics: Priciples and Practice*. Addison-Wesley Publishing Company, second edition, 1990.

[29] S. Nakajima, H. Atsumi H, R. Kikinis, T. M. Moriarty, D. C. Metcalf, F. A. Jolesz, and P. M. Black. Use of cortical surface vessel registration for image-guided neurosurgery. *Neurosurgery*, 40(6), 1997.

[30] Michel A. Audette, K. Siddiqi, and T. M. Peters. Level-set surface segmentation and fast cortical range image tracking for computing intrasurgical deformations. *LNCS: Medical Image Computing and Computer-Assisted Intervention*, 1679, 1999.

[31] P. J. Besl and N. D. McKay. A method for registration of 3-d shapes. *IEEE Transactions on Pattern Analysis and Machine Intelligence*, 14(2), February 1992.

[32] William M. Wells, Paul Viola, Hideki Atsumi, Shin Nakajima, and Ron Kikinis. Multimodal volume registration by maximization of mutual information. *Medical Image Analysis*, 1(1):35–51, 1996.

[33] K. S. Arun, T. S. Huang, and S. D. Blostein. Least-squares fitting of 2 3-d point sets. *IEEE Transactions of Patter Analysis and Machine Intelligence*, 9(5):699–700, 1987.

[34] C. E. Shannon. A mathematical theory of communication. *Bell System Technical Journal*, 27:379–423 and 623–656, 1948.

[35] D. L. Hill, C. Studholme, and D. J. Hawkes. Voxel similarity measures for automated image registration. pages 205–216. SPIE: In Proceedings of the Third Conference of Visualization in Biomedical Computing, 1994.

[36] Paul Viola and William M. Wells. Alignment of maximization of mutual information. *International Journal of Computer Vision*, 24(2):137–154, 1997.

[37] A. Collignon, F. Maes, D. Delaere, D. Vandermeulen, P. Suetens, and G. Marchal. *Automated Multimodality Image Registration Based on Information Theory*. Kluwer Academic Publishers, Dordrecht, 1995.

[38] Colin Studholme, D. L. G. Hill, and D. J. Hawkes. An overlap invariant entropy measure of 3d medical image alignment. *Pattern Recognition*, 32(1):71–86, 1999.

[39] Frederik Maes, Andre Collignon, Dirk Vandermeulen, Guy Marchal, and Paul Suetens. Multimodality image registration by maximization of mutual information. *IEEE Transactions on Medical Imaging*, 16(2):187–198, April 1997.

[40] M. A. Audette, F. P. Ferrie, and T. M. Peters. An algorithmic overview of surface registration techniques for med. imag.. *Medical Image Analysis*, 4:201–217, 2000.

[41] A. E. Johnson and S. B. Kang. Registration and integration of textured 3d data. *Image and Vision Computing*, 17(2):135–147, 1999.

[42] David M. Cash, Tuhin K. Sinha, Will C. Chapman, Robert L. Galloway, and Michael I. Miga. Fast accurate surface acquisition using a laser scanner for image-guided surgery. SPIE: Med. Imag. 2002, 2002.

[43] M. Rioux. Visual information technology. website: www.vit.iit.nrc.ca.

[44] J. H. Friedman, J. L. Bentley, and R. A. Finkel. An algorithm for finding best matches in logarithmic expected time. *ACM Transactions on Mathematical Software*, 3(3):209–226, 1977.

[45] D. Mount. Ann programming manual. website: www.cs.umd.edu/m̃ount/ANN, 1998.

[46] William H. Press, Saul A. Teukolsky, William T. Vetterling, and Brian P. Flannery. *Numerical Recipies in C : The Art of Scientific Computing*. Cambridge University Press, second edition, 1993.

[47] S.J. Ahn, W. Rauh, and H.-J. Warnecke. Least-squares orthogonal distances fitting of circle, sphere, ellipse, hyperbola, and parabola. *Pattern Recognition*, 34(12):2283–2303, 2001.

[48] V. R. Mandava, J. M. Fitzpatrick, C. R. Maurer, and et al. Registration of multimodal volume head images via attached markers. In *Medical Imaging IV: Image Processing*, volume 1652, pages 271–282. SPIE, 1992.

[49] Richard O. Duda, Peter E. Hart, and David G. Stork. *Pattern Classification*. Wiley-Interscience, 2 edition, 2001.

[50] Alfred Renyi. *Probability Theory*. North Holland Publication Co., 1970.

[51] Solomon Kullback. *Information Theory and Statistics*. Wiley, 1959.

[52] F. Glover. Tabu search: A tutorial. *Interfaces*, 20(4):74–94, 1990.